15th International Workshop on THERMAL INVESTIGATIONS OF ICS AND SYSTEMS
7-9 October 2009, Leuven, Belgium

Hot Spot Targeting with a Liquid Impinging Jet Array Waterblock

D. Nikolić, M. Hutchison, P.T. Raide, A.J. Robinson
Department of Mechanical & Manufacturing Engineering
Trinity College Dublin
Dublin 2, Ireland

***Abstract*-Liquid cooling of electronic devices is widely accepted as the next logical step for electronics thermal management as board level air cooling becomes insufficient to meet the needs of next generation components and devices. One promising technology is liquid jet array impingement as it can achieve exceptionally high area averaged heat transfer coefficients. In this work the use of arrays of liquid impinging jets in a waterblock configuration is posed as one possible technology for on-chip hot spot targeting. A simple test case is posed and an optimization strategy is employed to distribute jets in the hot spot and outer regions differently in order to reduce the maximum temperature difference and/or the root mean squared deviation of the temperature on the chip. It is concluded that with a priori knowledge of the heat flux distribution on-chip, this method of hot spot targeting offers an uncomplicated and potentially cost effective means of bulk cooling and temperature homogenization.**

I. INTRODUCTION

The increase in device density and clock speeds in electronic components and devices has led to escalating demand for dissipation of the waste heat generated by the active devices. In many applications the power densities far exceed the capabilities of conventional low-tech fan-finned heat sinks. This is due to several constraining issues which includes, but is not limited to, fin efficiency, fan acoustic emissions, fan power consumption and electronic packaging/miniaturization issues. A further issue is that devices operating at moderate overall power can in some cases generate local hot spots with power densities in the order of kW/cm^2 [1]. For example, Figure 1 shows a thermal image of hot spots generated on a Pentium 4 2.8GHz in a desktop PC. To obtain this image a purpose built liquid cooler was fabricated in which the CPU is cooled by IR transparent oil (Fluka 69808) flowing within a 1.0 mm channel sandwiched between the CPU and a ZnSe IR transparent window and IR images were collected with a FLIR 840 thermal imaging camera. For this case and others, if adequate thermal management is not provided, premature device failure can be expected either by direct failure of the semiconductor or more likely by progressive accumulation of thermomechanical damage and eventual cracking of interconnect structures [1].

Active liquid cooling shows very good potential for electronics thermal management of next generation electronic components. In particular, microfluidic devices such as microchannels and microjets can achieve exceptional overall heat transfer coefficients with very low energy consumption [2]. A very attractive benefit of liquid cooling is that if it is deployed in large numbers such as may be required for data centres, the heat energy, now stored in a liquid opposed to air, can easily be reused (e.g. for space or process heating), which reduces the overall combined energy consumption and carbon footprint of the scenarios.

As noted by Robinson [2] microjet arrays can provide exceptional temperature uniformity whereas microchannels are at a disadvantage on this point due to the singular direction of the microchannel flow which can cause large axial temperature gradients. Another beneficial aspect of impinging jets is that the jet orifices can be arranged strategically to concentrate jets in areas of high local heat flux which makes them ideal for hot spot targeting whereas microchannels are a more global cooling strategy.

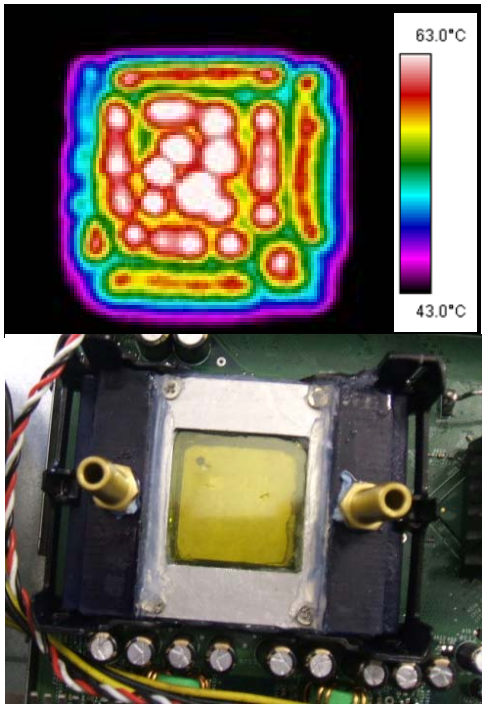

Fig. 1. Top: Thermal image of hot spot generated on the CPU of a conventional desktop PC. Bottom: IR transparent liquid minichannel heat sink.

 ISBN: 978-2-35500-010-2

In this work, the Nusselt number correlation recently developed by Robinson and Schnitzler [3] is implemented to investigate the feasibility of hot spot targeting using submerged liquid jet arrays. The case under consideration is a waterblock heat sink opposed to direct liquid cooling. A waterblock-type of heat sink is preferable for many reasons since the heat sink does not need to be integrated into the electronics package which would increase the cost and complexity of the system, albeit at a disadvantage with regard to thermal performance since it will still require a thermal interface material between in and the electronic component. The waterblock alternative is also a pluggable solution making it suitable for retrofitting existing systems.

II. LIQUID JET ARRAYS

A. Thermal Hydraulics of Impinging Liquid Jet Arrays

There are surprisingly few correlations available for predicting the heat transfer and pressure drop characteristics of liquid impinging jet arrays although some do exist for both free jets [3 4, 5, 6] and submerged jets [3, 5]. The Robinson-Schnitzler correlation for the confined submerged scenario will be used in this work as it was developed for large numbers of confined and submerged liquid jets arranged in arrays, it considers variations in jet Reynolds number, jet-to-target spacing as well as the jet-to-jet spacing and also included information about the pressure drop characteristics. The correlation is,

$$\frac{Nu_L}{\Pr^{0.4}} = 23.39\,\mathrm{Re}_{d_n}^{0.46}\left(\frac{S}{d_n}\right)^{-0.442}\left(\frac{H}{d_n}\right)^{-0.00716} \quad (1)$$

which is valid for jet to target spacings of $2 \le H/d_n \le 3$ and interjet spacings of $3 \le S/d_n \le 7$. Since low hydraulic pumping power is crucial for energy efficient water cooled devices, Robinson and Schnitzler also developed a correlation for the friction factor as,

$$f = 0.51 + \frac{229.9}{\mathrm{Re}_{dn}} \quad (2)$$

which agreed with a previous correlation developed in [6], albeit strictly for free jet arrays. With regard to the pressure drop and pumping power, Whelan and Robinson [7] showed that simple modifications to the inlet geometry can reduce the pressure drop without significantly affecting the heat transfer.

B. Liquid Jet Array Waterblock Concept

One embodiment of the liquid jet array waterblock concept is illustrated in Fig. 2. The main performance indicator of this type of waterblock cooler is that it can achieve exceptional heat transfer with very low hydraulic pumping power. Compared with other commercially available waterblocks, which almost invariably use low velocity water impinging onto miniature surface extensions machined into copper, this concept achieves the desired thermal resistance by using tens to thousands of high velocity jets which impinge on a flat copper surface. Since the main body of the waterblock is easily manufactured from plastic by injection molding, it is envisaged that this waterblock will be very inexpensive compared with the competition which require CNC micromachining of complex features which adversely affects overall cost. For a target thermal resistance, increasing the number of jets, i.e. by decreasing the jet orifice diameter, causes the pumping ower to continually decrease. However, there are practical limits such as jet clogging and manufacturability which limit the minimum size of the jets.

The waterblock illustrated in Fig. 2 operates as follows; water enters the foremost port shown in Fig. 2 and flows through a section of internal tubing into a lower plenum. The water stagnates in this plenum section and is then forced across the jet nozzle plate through which many miniature to micro-sized jet orifices are situated. The jets impinge upon the topside of a copper plate whose lower face is in thermal communication with the electronic component via a layer of thermal interface material (not shown). Subsequent to impinging on the surface the jets are forces laterally outward and exit at four channels at the outer edges of the impingement zone. The water is then forced to flow upward along the side channels into an upper collection chamber and subsequently forced out of the device to a remote heat exchanger through the rear exit port shown in Fig. 2. The waterblock housing was designed in a 3-D CAD package and subsequently printed using a 3D Systems InVision™ 3D Printer.

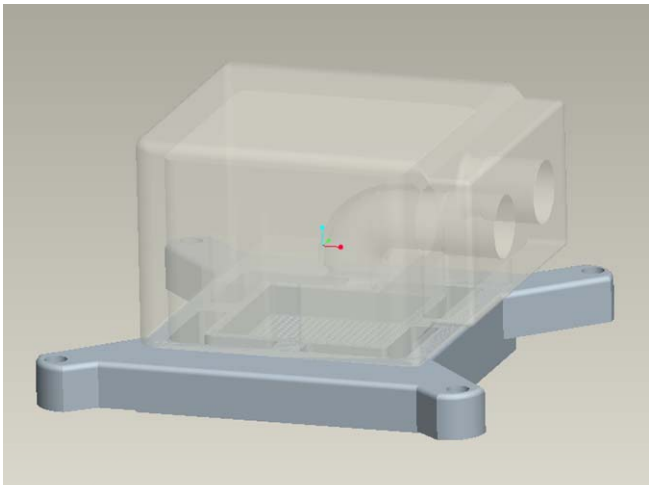

Fig. 2. Impinging jet waterblock concept drawing.

C. Prototype Waterblock Testing

A simple test facility has been commissioned in order to obtain the relevant thermal hydraulic measurements for testing different waterblock design concepts. To simulate an active electronic device a copper block with exposed surface area of 28.7 mm x 28.7 (commensurate with a Pentium 4 CPU) was imbedded in a block of nylon which provided insulation as well as a rigid body for mounting the waterblocks. The copper block was fitted with two cartridge heaters with a total combined power of 350W as well as three thermocouples near the upper exposed face in order to monitor the surface heat flux. These thermocouples also facilitated the extrapolation of the surface temperature.

The test facility also included an instrumented flow delivery system in which the plumbing components (pumps,

 ISBN: 978-2-35500-010-2

hosing fittings etc.) were 'off the shelf' from popular electronics cooling equipment distributors. The flow loop consisted of a Laing DD12V-D5 variable speed pump which drew deionized water from a 1.5L water reservoir manufactured by Danger Den. In order to monitor the flow rate, a rotameter, with a flow range of 2-10 LPM ± 1.5% FS, was installed within the system. Two 1.5 mm diameter sheathed T-type thermocouples, coupled with Fluke54II Thermometers (±0.3°C), were used to measure and record the water temperatures at the inlet and outlet of the water block as well as the outlet of the remote heat exchanger. Pressure taps were installed on either side of the water block to measure the pressure drop with a Digitron 2083P (0-200 kPa ± {0.1% rdg + 0.1% FS}) differential pressure meter. The heat absorbed by the waterblock was dissipated to the room air by a Thermochill PA120 remote heat exchanger fitted with a Yate Loon D12SH-12 fan.

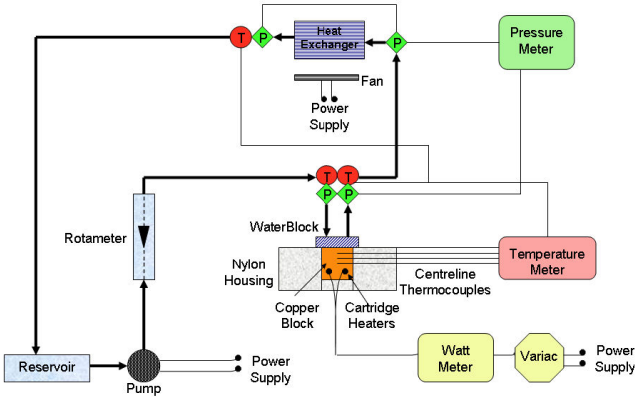

Fig. 3. Test facility for water block characterization.

The waterblock was fixed to the instrumented copper block with a layer of thermal grease sandwiched between them. As it is cumbersome to continuously measure the thermal resistance of the TIM layer which can change from test-to-test, a 50 µm wire diameter bare thermocouple was fastened to the lower face of the waterblock so that the average surface heat transfer could be calculated without having to subtract out the thermal resistance of the TIM

Fig. 4 shows a adequate comparison of predicted thermal resistance versus experimental measurements for an array of of 0.3 mm jets with a density of 81 jets/cm^2.

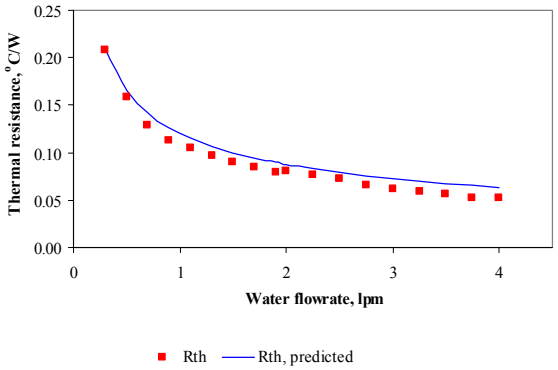

Fig. 4. Measured and predicted heat transfer performance.

III. HOT SPOT TARGETING

A. Problem Statement

The evaluate the efficacy of hot spot targeting using an impinging liquid jet array waterblock a simple test case was selected. Here a 50mm x 50mm overall surface area is chosen with one hot spot which is chosen arbitrarily, as depicted in Fig. 5. The lower face of a copper block is exposed to this heat source, representing an electronic component. The imposed heat flux at the hot spot reaches 200 W/cm^2 while in other areas is uniform at 30 W/cm^2. The heat is transferred by conduction through the copper slab, including the influence of lateral heat spreading. The opposite side of the copper block, depicted in the far right diagram in Fig. 5, is exposed to three different cooling scenarios:

Case I: Cooling using some traditional method, for instance an efficient heat sink with forced convection, with constant thermal resistance of 0.1 K/W.

Case II: Cooling by only one impingement jet array covering the whole copper block area.

Case III: Tailored cooling by applying two impingement jets configurations: one focussed at the hot spot and the second cooling the rest of the heated surface.

The performance indicators by which each method is evaluated are the maximum temperature and the temperature uniformity of the bottom surface of the copper i.e. the electronic component.

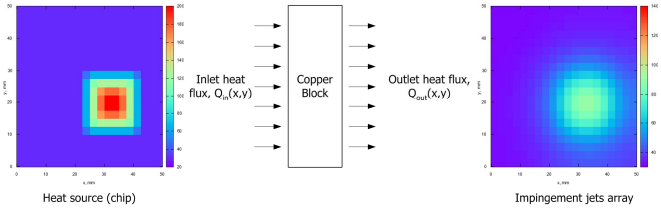

Fig. 5. The hot spot targeting problem.

B. Modelling Framework

The problem posed here is simply the solution to the steady 3D energy equation within the solid copper block, given as,

$$\frac{\partial^2 T}{\partial x^2}+\frac{\partial^2 T}{\partial y^2}+\frac{\partial^2 T}{\partial z^2}=0 \qquad (3)$$

Equation 3 was solved using the finite difference technique with second order approximations of the spatial derivatives. Along the four edge boundaries adiabatic boundary conditions were applied. At the bottom boundary a distributed heat flux boundary condition was imposed,

$$-k\left.\frac{\partial T}{\partial z}\right|_{z=0}=Q_{in}(x,y) \qquad (4)$$

where Q_{in} is spatially distributed according to the profile illustrated in Fig. 5. On the opposite face a convective boundary condition was imposed which depended on the scenario under consideration. For Cases I and II the thermal resistance is spatially uniform so that the boundary condition is simply,

 ISBN: 978-2-35500-010-2

$$-k\left.\frac{\partial T}{\partial z}\right|_{z=L} = h[T(x,y,L)-T_\infty] \qquad (5)$$

where h can be considered an effective thermal conductance for Case I and the surface averaged heat transfer coefficient for Case II and T_∞=25°C which is held fixed for all scenarios for comparison purposes. For Case III the situation is somewhat more complex since there are two different jet configurations with different surface averaged heat transfer coefficients which can be expressed in the form,

$$-k\left.\frac{\partial T}{\partial z}\right|_{z=L} = \begin{cases} h_i[T(x,y,L)-T_\infty] & inner\ jets \\ h_o[T(x,y,L)-T_\infty] & outer\ jets \end{cases} \qquad (6)$$

where the jets are configured such that h_i>h_o in order to provide preferential cooling in the region of high heat flux so as to create a more uniform temperature distribution on the simulated electronic component.

C. *Base Case Scenario*

To begin, base case scenarios for the Cases I, II & III have been posed in order to gain a general feel for their performance characteristics as well as providing the starting points for a preliminary optimization strategy for minimizing the temperature non-uniformities for Cases II & III. The base case considered for Case I is a conventional heat sink with a uniform thermal resistance of 0.1 K/W. This corresponds with an effective thermal conductance of h=4000W/m^2°C or a specific thermal resistance of R''_{th}=2.5x10^{-4} m^{2}K/W, which can be considered a very high performance fan assisted heat sink. For Case II the base case was selected which populates the nozzle plate with 0.5 mm orifices with a dimensionless interjet spacing of S/d_n=2.5 and jet-to-target spacing of H/d_n=2.5. The total volumetric flow rate was initially selected to be 3.5 LPM which resulted in a net surface averaged heat transfer coefficient of h=21,296 W/m^2°C (R''_{th} =4.696x10^{-5} m^{2}K/W). For Case III the jet size and layout was kept identical to that of Case II although two separate regions are considered. In the low heat flux the total flow rate was reduced so as to achieve the same surface averaged heat transfer coefficient as in Case II. For illustrative purposes the net flow rate through the inner hot spot region jets was increased to achieve a surface averaged heat transfer coefficient of h=62,490 W/m^2°C (R''_{th} =1.600x10^{-5} m^{2}K/W) in this region. The same net effect could have been achieved by populating the nozzle with more jets of smaller diameter though this is inconvenient with regard to a starting point for an optimization strategy.

Thermal performance indicators of the three base case scenarios are illustrated in Fig. 6 and 7. On the far left of Fig. 6 as well as in Fig. 7 it is clear that the maximum temperature in the vicinity of the hotspot for the Case I cooling solution (top) approaches 170°C which far exceeds the typical maximum allowable temperature, which is of the order of 100°C. The accompanying heat flux distribution at the top surface shown in the left figure indicates strong lateral conduction within the copper block as it acts as a heat spreader since the heat sink in this case is not a strong one. For the uniform jet configuration (Case 2: middle of Fig. 6) the cooling performance is drastically improved with the maximum surface temperature dropping to about 80°C, which is acceptable, and almost doubling of the maximum heat removal rate on the back face as the impinging jets are a much stronger heat sink compared with the previous scenario. As such there is reduced lateral conduction and heat spreading within the copper as depicted in the middle right plot in Fig. 6. Even still, Figs. 6 and 7 indicate that there are still notable temperature non-uniformities as the temperature in the outer regions is about 40°C representing a maximum to minimum temperature differential of $\Delta T_{max}=T_{max}-T_{min}\sim$ 40°C.

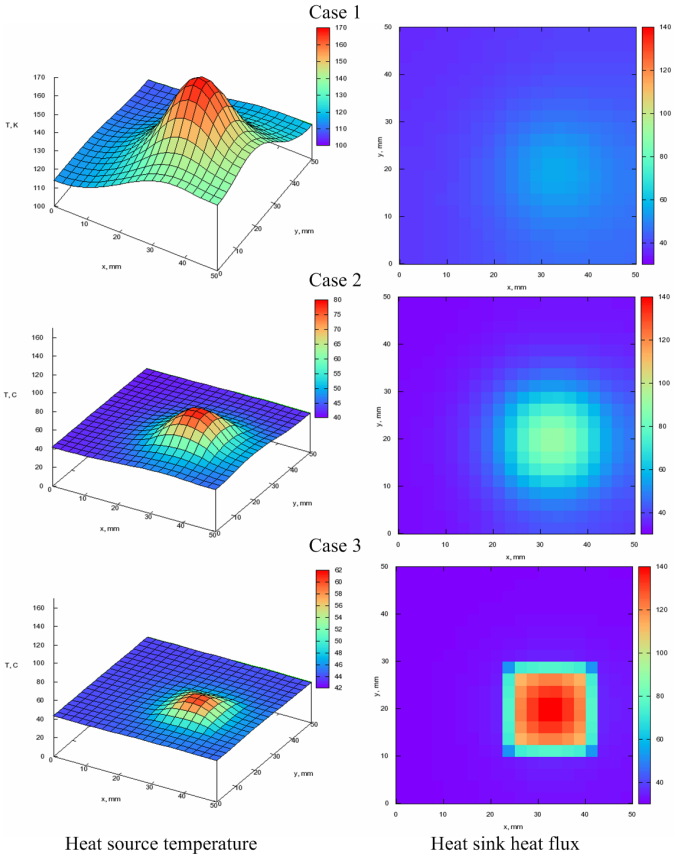

Fig. 6. Thermal performance indicators of the three scenarios for cases under consideration.

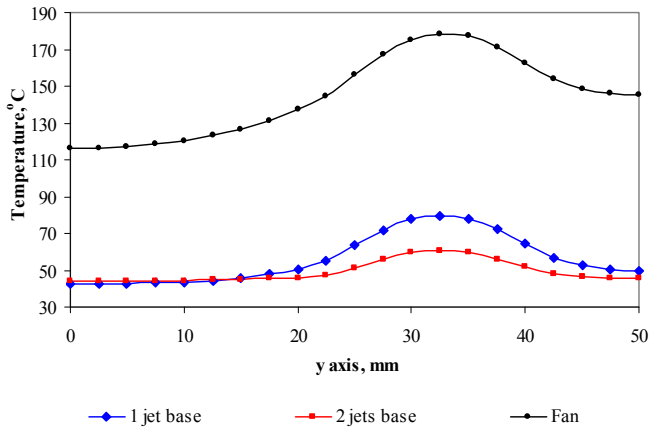

Fig. 7. Comparison of temperature profiles through the centreline of the hot spot zone (Base cases I, II and III).

 ISBN: 978-2-35500-010-2

For base Case III the jet cooling is now concentrated at the hot spot and it is evident that not only has the maximum temperature diminished to ~60°C due to the high heat removal rates in this region, but so also has the magnitude of the thermal gradients at the heat source as represented by T_{max}-T_{min}~ 20°C. These are both desirable outcomes with regard to component performance and reliability.

D. *Optimization of Jet Cooling*

The next logical step is to attempt to further improve the performance of impingement jet array configurations by reducing the difference between the highest and the lowest temperature, $\Delta T_{max}=T_{max}-T_{min,}$ whilst maintaining the maximal temperature, T_{max}, under the given threshold. This should be a simple method which could distribute temperatures more uniformly along the surface. As a first approximation an uncomplicated measure of the quality of the temperature distribution was chosen to be the deviation from the average value as given by the normalized root mean square deviation (NRMSD) given as,

$$NRMSD = \frac{RMSD}{T_{msx} - T_{\min}} \qquad (7)$$

where the root mean square deviation (RMSD) is given by,

$$RMSD = \frac{\sqrt{\sum (T(x,y) - \overline{T})^2}}{N_{po\,int\,s}} \qquad (8)$$

The average temperature on the surface is,

$$\overline{T} = \frac{\sum_{x=0,y=0}^{x=1,y=1} T(x,y)}{N_{po\,int\,s}} \qquad (9)$$

and the number of points are,

$$N_{po\,int\,s} = (N_x + 1)(N_y + 1) \qquad (10)$$

Based on the abovementioned requirements, the problem can be formulated as the minimization of the NRMSD for given maximal allowed temperature and given maximal allowed temperature difference while optimizing design (d_n, s, h) and operating parameters (V_{H20}). Thus, the mathematical formulation of the problem for Case II involves minimizing the NMRSD using the appropriate heat transfer correlation (Eq. 1). The design and operating parameters space (which were selected based on practical manufacturing considerations) is given by; $d_n \in [0.3, 1.5]$ mm, $h/d_n \in [2, 3]$, $s/d_n \in [2.2, 7]$, $V_{H2O} \in [0.1, 50]$ LPM and the constraints $T_{max}=\{60, 70, 80\}$°C are implemented to investigate the influence of the maximum target operating temperature.

The results are illustrated in Fig. 8 for a cross section through the hot spot zone. Table 1 shows the design and operating parameters for each case. Since this is a global cooling strategy i.e. the surface averaged heat transfer coefficient is uniform for each scenario, the maximum allowable temperature is achieved though the temperature profiles still show significant non-uniformity in the region of the hot spot. Some improvement in the temperature uniformity is observed for decreasing T_{max} as evident in Table 1 where both the RMSD and ΔT_{max} tend to decrease with decreasing T_{max}.

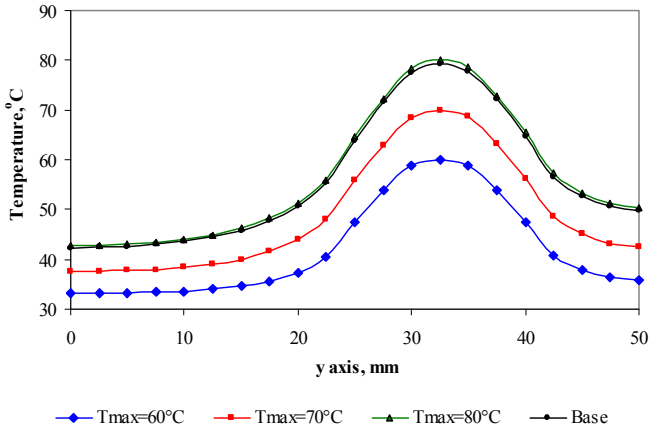

Fig. 8. Comparison of optimal and base case temperature profiles through the centreline of the hot spot zone (Case II)

TABLE I
Optimization results for Case II

Property	$T_{max}=80^0$C	$T_{max}=70^0$C	$T_{max}=60^0$C
RMSD, ^{0}C	8.097	6.891	5.546
ΔT_{max}, ^{0}C	37.89	32.76	26.87
d_n, mm	0.426	0.403	0.300
h/d_n	2.41	2.38	2.23
s/d_n	2.87	2.98	3.55
V_{H2O}, LPM	2.372	4.914	8.958
R''_{th}, m^{2}K/W	4.825E-5	3.288E-5	1.954E-5
Q_{pump}, W	0.0102	0.0634	0.6978

In Case III the problem is formulated in a similar manner as in Case II except the design and operating parameters of the inner hot spot zone and the outer region can be varied independently. The results are presented in Fig. 9 and Table 2. Comparing Figs. 8 & 9 and Tables 1 & 2 it is evident that this simple technique of modifying the jet configuration in the hot spot region improves the temperature uniformity both by decreasing the RMSD from ~ 7°C down to ~1.4°C as well as decreasing ΔT_{max} from ~ 30°C down to ~9.5°C. Even still there exists a temperature rise in the hot spot region since T_{max} is a constraint which occurs at the peak heat flux of the hot spot and $\overline{T}$ is used in Eq. 8. As a result, relaxing the heat transfer in the outer region is not feasible within the constraints of the optimization strategy adopted in this particular scenario. However, additional simulations were performed whereby T=55°C and 60°C were used instead of $\overline{T}$ in Eq. 8. The results are presented in Fig. 10 and 11 for the case of T_{max}=60°C. It is evident that for these two cases the surface averaged temperature increases as expected. Nevertheless, the temperature uniformity, quantified here in terms ΔT_{max} and RMSD, tends to improve, in particular for the 55°C case. For the 60°C case the RMSD tends to worsen as a result of the depression in the temperature distribution at the edge of the hotspot.

The temperature depressions occur since the assumed hot spot is a piece-wise continuous function increasing from 30W/cm^2 in the outer region to 200W/cm^2 at the peak of the hot spot. At the hot spot there is a step change (increase) in the surface averaged heat transfer coefficient on the opposite face of the copper block which causes local minima to occur

 ISBN: 978-2-35500-010-2

in the temperature distribution which in turn induces lateral heat flow within the copper slab. Since the specific thermal resistance in the hot spot zone is largely determined by the requirement that T_{max}=60°C and does not vary considerably for each scenario in Fig. 10, decreasing the specific thermal resistance in the low heat flux region, i.e. increasing the averaged surface temperature, causes the local minima to become progressively more pronounced. This occurs to the point that the RMSD tends to be largest for the highest averaged surface temperature even though ΔT_{max} is lowest.

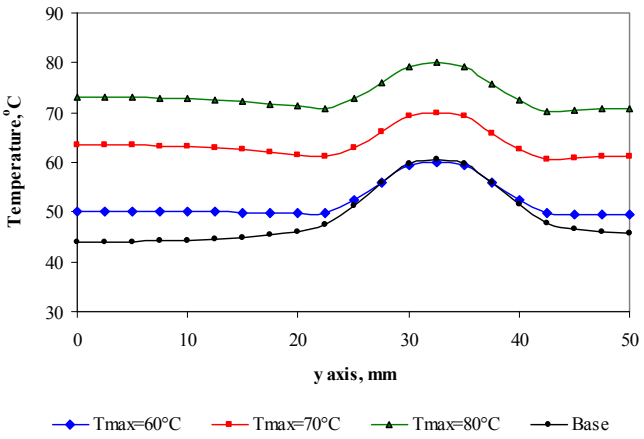

Fig. 9. Comparison of optimal and base case temperature profiles through the centreline of the hot spot zone (Case III).

TABLE II
Optimization results for Case III

Property	T_{max}=80°C	T_{max}=70°C	T_{max}=60°C
RMSD, °C	1.446	1.387	1.304
ΔT_{max}, °C	9.84	9.48	8.97
Inner Jets			
d_n, mm	1.176	0.422	0.306
h/d_n	3.00	2.41	2.23
s/d_n	3.23	2.84	3.482
Q_{pump}, W	0.1445	0.0803	0.5305
R''_{th}, m^2K/W	2.738E-5	2.042E-5	1.355E-5
Outer Jets			
d_n, mm	0.795	0.703	0.668
h/d_n	2.31	2.64	2.73
s/d_n	2.467	2.56	2.448
Q_{pump}, W	0.1445	0.0002	0.0007
R''_{th}, m^2K/W	1.568E-4	1.237E-4	9.095E-5

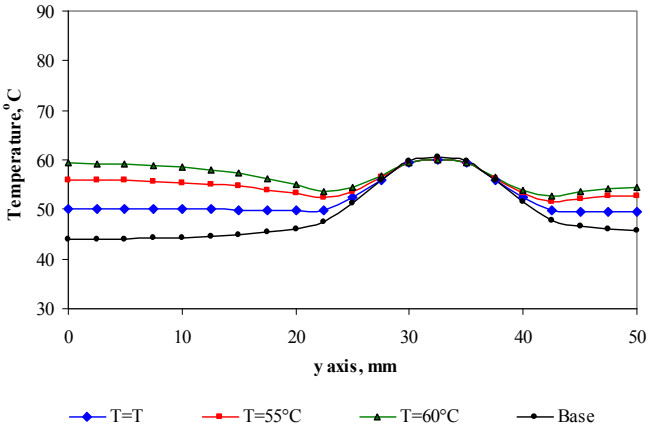

Fig. 10. Temperature profiles through the centreline of the hot spot zone (Case III).

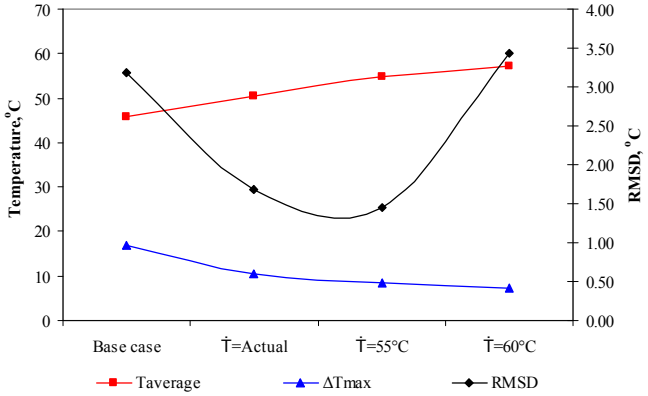

Fig. 11. Performance indicators for different average surface temperatures

IV. CONCLUSIONS

An uncomplicated technique of using impinging jet arrays of different configuration within a waterblock has been shown to predict improvement in the temperature uniformity of an electronic component with a single hot spot. Future work should involve the characterizing hot spots for real devices, perhaps using the IR thermography techniques.

ACKNOWLEDGMENT

The authors acknowledge Roger Kempers (Alcatel-Lucent) and John Mullins (Bell Labs Ireland) for rapid prototyping the waterblocks.

REFERENCES

[1] DTI Global Watch Mission Report, "Developments and trends in thermal management technologies - a mission to the USA," December 2006.

[2] A. J. Robinson, "A Thermal-Hydraulic Comparison of Liquid Microchannel and Impinging Liquid Jet Array Heat Sinks for High Power Electronics Cooling," *IEEE Transactions on Components and Packaging Technologies*, in press.

[3] A.J. Robinson, E. Schnitzler, "An Experimental Investigation of Free and Submerged Liquid Miniature Jet Array Impingement Heat Transfer", *Experimental Thermal and Fluid Science*, vol. 32, pp. 1-13, 2007.

[4] Y. Pan, B.W. Webb, "Heat transfer characteristics of arrays of free-surface liquid jets," *Journal of Heat Transfer*, vol. 117, pp. 878-883, 1995.

[5] D.J. Womac, F.P. Incropera, S. Ramadhyani, "Correlating equations for impingement cooling of small heat sources with multiple circular liquid jets," *Journal of Heat Transfer*, vol. 116, pp. 482-486, 1994.

[6] M. Fabbri, V.K. Dhir, "Optimized heat transfer for high power electronics cooling using arrays of microjets," *Journal of Heat Transfer*, vol. 127, pp. 760-769, 2005.

[7] B.P. Whelan, A.J. Robinson, (2009) "Nozzle Geometry Effects in Liquid Jet Array Impingement", Applied Thermal Engineering, 29 (11-12), pp. 2211-2221.

 ISBN: 978-2-35500-010-2